The effect of dissolution, migration and precipitation of platinum in Nafion®-based membrane electrode assemblies during fuel cell operation at high potential

Jennifer Péron, Yannig Nedellec, Deborah J. Jones*, Jacques Rozière

Institut Charles Gerhardt de Montpellier, UMR CNRS 5253, Laboratoire des Agrégats, Interfaces et Matériaux pour l'Energie, Université Montpellier 2, 34095 Montpellier Cedex 5, France

ABSTRACT

MEAs comprising Nafion® perfluorosulfonic acid-type membranes have been submitted to accelerated ageing operation conditions at high cell voltage, and characterised during the course of time in terms of gas consumption, gas crossover, and water production at the anode and cathode. Aged and end-of-life MEAs have been characterised using atomic force and scanning electron microscopy with energy dispersive analysis by X-ray spectroscopy, as well as transmission electron microscopy. A representative sample has been examined using X-ray photoelectron spectroscopy to identify the nature of the platinum species present in the membrane. Under high cell potential, platinum dissolves from the cathode, and migrates through ion-exchange sites in the membrane through a concentration effect. On encountering crossover hydrogen, platinum precipitates within the membrane as dispersed particles that comprise a metallic core and a shell of oxidised platinum. Platinum charged species act as centres for the generation of free radicals that chemically degrade the membrane, leading to increased porosity, gas crossover and ultimately membrane and MEA failure. Mass spectroscopic analysis of water generated even at open circuit has enabled identification of degradation fragments, the nature of which points to degradation both at polymer end groups, and functionalised pendant groups.

© 2008 Elsevier B.V. All rights reserved.

1. Introduction

The sharp increase in research in the field of proton exchange membrane (polymer electrolyte) fuel cells (PEMFC) over the past 15 years or so has been marked by the search for new membrane, catalyst and catalyst support materials giving increased fuel cell performance at lower cost [1–4]. Long-term performance data under conditions relevant to the intended use remain scarce, partly for reasons of the resource-intensive character of such tests, but also due to lack of reproducibility, for it is increasingly clear that component ageing and degradation processes are major issues in the durability of fuel cell operation, as described in two recent excellent review articles [5,6]. For automotive application, the high cell potential at open circuit typical of idling conditions is particularly harsh, well-known to accelerate the failure of membrane-electrode assemblies (MEAs), ultimately by membrane perforation [7]. Various local situations within a given MEA can lead to a localised high potential, and the effects of high potential phenomena will be implicated in membrane degradation even under nominally optimal operation conditions. Fuel cell operation under high potential is a means of accelerating ageing processes, in particular those induced electrochemically.

As long ago as 1988, researchers at the Mitsubishi Electric Corporation described potential-dependent dissolution of platinum from the cathode of phosphoric acid fuel cells (PAFC), and its mobility under high cell voltage leading to its transfer to the anode and identification of Pt in the electrolyte matrix [8]. It seems surprising, but it is only recently that similar events have been diagnosed for PEMFC, although platinum particle ripening effects at both anode and cathode were observed in the electrodes of MEAs submitted to long-term testing [9]. Ferreira et al. have reported formation of dissolved Pt species from a Pt/C electrocatalyst in $0.5\,M\,H_2SO_4$ at $80\,°C$ at an applied potential of 0.9–1.1 V, and further suggested that formation of soluble Pt species plays an important role in nanometer-level coarsening of Pt particle size in PEMFC electrodes and in micrometer-scale migration and subsequent precipitation of Pt in the cathode ionomer phase [10]. Recent studies have reported the presence of a Pt front precipitated within the membrane itself during operation under OCV [11,12] or potential cycling [13]. Cobalt has also been observed to leach from PtCo alloys catalysts and

* Corresponding author. Tel.: +33 467 14 3330; fax: +33 467 143304.
E-mail address: Deborah.Jones@univ-montp2.fr (D.J. Jones).

diffuse into Nafion® after operation of an MEA at constant 1 A cm^{-2} load [14]. Fluoride emission into drain water is a recognised means of detecting the attrition of perfluorosulfonic acid membrane types, as reported by Healy et al. [15], Curtin et al. [7], Mittal et al. [16] and others. Other recent work relates the fluoride emission rate (FER) under OCV operation to an increase in gas crossover and to the formation of hydrogen peroxide, also detected in drain water by an enzyme-based detection method [17] and within the electrolyte membrane by an electrochemical method [18]. Ex situ chemical degradation using a Fenton (H_2O_2/Fe^{2+}) medium [15] or gaseous H_2O_2 [19,20] have found value less as a method to predict MEA lifetime, than as a means of relating degradation phenomena occurring in situ to those initiated ex situ by a free radical or oxidative mechanism. Absolute MEA lifetime under OCV conditions depends on a number of factors, including the nature of the polymer backbone, side-chain and end groups, the composition and structure of the electrodes, which can affect assembly conditions, as well as temperature and relative humidity. Our contribution to this burgeoning field lies in this overall context, and below we describe a relation between an increase in membrane permeability, hydrogen and oxidant consumption and water generation at anode and cathode at open cell voltage, and the presence of Pt precipitated within Nafion® membrane-based MEAs as discrete particles, aggregated clusters or as an agglomerated band. We also provide irrefutable evidence for the presence of ionic platinum as Pt(II) and Pt(IV) in the membrane and attempt to understand the differences in the detrimental impact on membrane failure mechanism brought by the presence of this platinum compared with the recent work of Watanabe, in which particles of metallic platinum dispersed in Nafion membranes are found to lower fluoride emission from Nafion [21].

2. Experimental

2.1. MEA preparation

Membrane-electrode assemblies comprising Nafion®-112 (EW 1100 g mol^{-1}, thickness 50 μm) and electrodes supplied by Johnson–Matthey (0.4 mg Pt cm^{-2} and Nafion ionomer loading of 0.65 mg cm^{-2}) were prepared by pressing at 2 MPa for 10 mn, while increasing the temperature from ambient to 130 °C, followed by a 10 mn hold at 130 °C, before releasing pressure and lowering temperature. The graphite plates have serpentine flow fields, and H_2 and O_2 are fed in co-flow. Prior to assembly, as-received Nafion®-112 was treated by (i) immersion in boiling 3 wt% H_2O_2, followed by deionised water washing, (ii) immersion (30 mn) in 50 wt% HNO_3 at room temperature, followed by extensive washing with deionised water, (iii) boiling in H_2SO_4 (1 mol dm^{-3}) for 1 h, followed by water washing. Thereafter, membranes were stored in H_2SO_4 (0.5 mol dm^{-3}). Before use, they were treated in boiling deionised water for 1 h.

2.2. Ageing under open cell voltage

The fuel cell test station was operated on hydrogen and oxygen, at 80 °C, 1/1 bar at anode/cathode. Experiments were performed with both hydrated and dry gases. To ensure that each MEA was capable of providing a stable baseline performance, each was operated at 0.4 A cm^{-2} for 24 h before switching to open circuit conditions for run times of 25, 50, 75, 100 h and thereafter up to end-of-life. The cell voltage at open circuit was then monitored with time and, in experiments fed with dry fuel and oxidant, the volume of water produced at the anode and cathode sides and the gas consumption upstream of the cell were monitored in dead-end mode. Hydrogen crossover current was measured in experiments in which

the oxidant was replaced by nitrogen at the cathode side using a potentiostat Autolab PGSTAT 12 with a scan rate of 5 mV s^{-1}. Gases were humidified at 30 °C during the measurement, and at 80 °C during OCV hold.

2.3. Analysis of product water

Water was produced at the anode and cathode on feeding the fuel cell with dry gases even under open cell voltage. Product water was collected and analysed for its fluorine content at the CNRS Service Central d'Analyse at Vernaison, France, and for the presence of charged degradation products using negative ion electrospray mass spectroscopy. A Waters Platform IIe apparatus was used for the latter using acetonitrile as solvent.

2.4. Atomic force and electron microscope characterization

Samples were examined using atomic force, scanning and transmission electron microscopies (AFM, SEM, TEM). For AFM and SEM, aged MEAs were embedded in a thermally curable epoxy resin, set by heating at 80 °C for 24 h. The surface parallel to the edge of the MEA around gas inlet, gas outlet and central MEA zones was polished with a diamond knife. The AFM was a Digital Nanoscope IIIA instrument, operated in tapping mode at room temperature in an air atmosphere. Using AFM, a platinum band of width 150 nm was observed (micrographs not shown), in agreement with the results from TEM described below. Two sets of SEM apparatus were used, a Cambridge S360 coupled to Energy Dispersive X-ray Spectroscopy (EDX) from Oxford Instruments ISIS 200 and an FEI Quanta 200 linked to Oxford Instruments INCA 300 EDAX. A JEOL 1200 EX II TEM apparatus was used, with observations on MEA samples embedded in resin and microtomed to give thin sections.

2.5. X-ray photoelectron spectroscopy

XPS spectra were recorded using a Physical Electronics PHI 5700 instrument and Mg Kα excitation ($h\nu$ = 1253.6 eV), equipped with a hemispheric electron analyser. Binding energies (BEs) were determined with an accuracy of ±0.1 eV. Charge referencing was measured against adventitious carbon (C 1s 284.8 eV). The residual pressure in the analysis chamber was maintained below 10^{-7} Pa during all measurements. Spectra were recorded on an aged MEA sample previously examined by SEM. Thus the resin-bound sample was inserted in the sample holder and successive cycles of argon abrasion and analysis were performed, in a first set of experiments starting from the anode side of the MEA and, in a second set of experiments, starting from the cathode side of the MEA. The resulting spectra were analysed and simulated using the Multipack programme from Physical Electronics.

3. Results and discussion

3.1. Cell voltage, gas consumption and water production under open circuit conditions

The response of the MEA to an applied current density of 0.4 A cm^{-2} at a cell temperature of 80 °C and gas humidification at 80 °C is shown in Fig. 1. Stable behaviour was observed over the 24 h validation period, with a cell voltage of 0.7 V. Once the load was removed however, a rapid decay within the ensuing 20–30 h was observed, while thereafter the cell voltage decreased more slowly until the MEA ultimately failed through an abrupt and catastrophic drop in cell voltage. A typical cell potential–time plot is shown in Fig. 1, where the lifetime under OCV was 185 h. Ensuing exper-
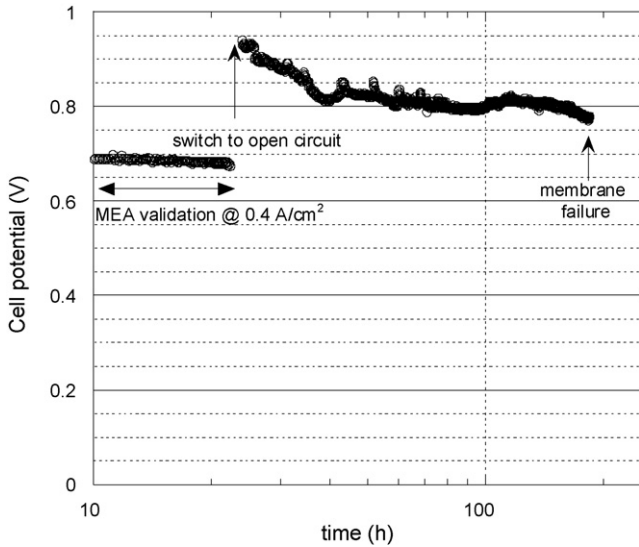
Fig. 1. Typical cell potential–lifetime plot at open circuit of a Nafion®-112-based MEA. H_2/O_2, 80 °C, anode/cathode 1/1 bar, full gas humidification.

Fig. 3. Water collected at anode (●) and cathode (■) of a Nafion®-112-based MEA maintained at open circuit voltage at 80 °C, H_2/O_2, no gas humidification, and ratio of water collected at cathode/anode (⊠).

iments described below enable interpretation of the processes occurring during both regimes of performance loss.

Using a fresh MEA prepared in the same way, the hydrogen crossover current was determined in a series of experiments for run times at open circuit voltage of 25, 50, 75, 100 h and up to end-of-life (ca. 250 h). In these measurements, the current required to electrochemically oxidise hydrogen gas that permeates directly from the anode side is measured. In general, for fuel cell membranes at beginning-of-life (BOL), the hydrogen crossover current density is in the range of 1–5 mA cm^{-2}, depending on the nature and thickness of the electrolyte membrane and hydrogen partial pressure, as well as temperature and relative humidity. In agreement with these general observations, the initial (BOL) hydrogen crossover current density in the present work is 1.5 mA cm^{-1}, however it increases with exponential dependence on time to reach 15 mA cm^{-2} after 250 h, Fig. 2. The result is consistent with that reported for an MEA aged under H_2/air by Inaba et al. [17]. The rate of performance degradation on air is less severe than occurs on oxygen and the increase in membrane permeability is correspondingly slower. The progressively higher current related to crossover hydro-
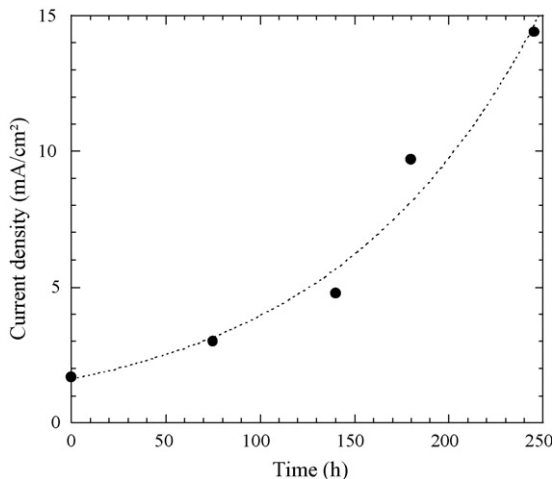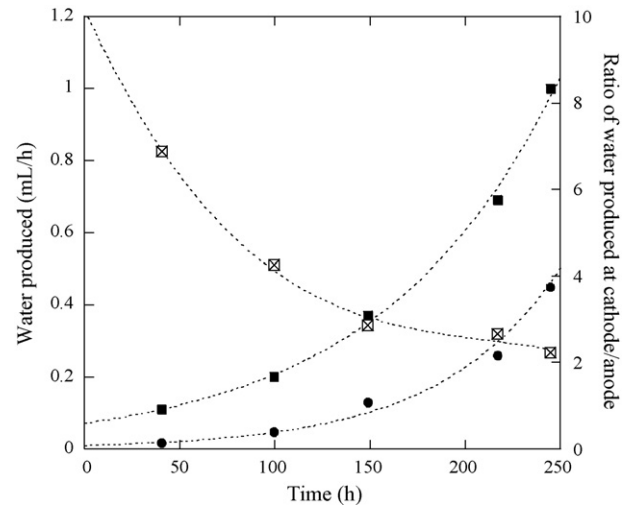
gen is clear indication of the increasing permeability of Nafion®-112 to hydrogen with time at open circuit. In addition, the slow increase in hydrogen crossover current during the first ca. 50 h at open circuit would tend to suggest that the rapid drop in cell voltage observed (Fig. 1) during this phase of ageing is not related to an increase in membrane permeability, but to other effects such as platinum dissolution or carbon corrosion, or the presence of contaminants. In contrast, the slower performance loss with time can find its origins in this phenomenon.

Even during experiments carried out with non-humidified gases at no applied load, water was produced at both anode and cathode. The amount of water collected at anode and cathode is plotted against the time at open circuit in Fig. 3. This production of water necessarily implies consumption of feed gases; this consumption is shown in Fig. 4 in experiments using dry (Fig. 4a) and hydrated (Fig. 4b) feed gases. The volume of product water at anode and cathode, and the consumption of non-hydrated hydrogen and oxygen all have exponential dependence on the time spent at open circuit voltage. However, when the gases are hydrated, the increase in gas consumption is more rapid such that an almost linear dependence is observed with time. Absorption of gases is higher in the hydrated membrane, which contributes to increased membrane permeability. In both cases, consumption of hydrogen is twice that of oxygen, which is consistent with the utilisation of these gases in forming water. The open circuit voltage for the MEA fed with dry gases is slightly higher than that when the H_2 and O_2 are hydrated, but the performance loss with time is similar and for both assemblies an irreversible drop in cell potential occurred after 200–250 h. In both cases dismantled MEAs are punctured in the gas inlet region where membrane permeability becomes highest, leading to uncontrolled direct reaction of hydrogen and oxygen.

According to Sakai et al. [22], the permeability of hydrogen and oxygen in Nafion®-125 membranes depends on the degree of hydration of the membrane. In the dry and wet states, the permeability of hydrogen is higher than that of oxygen by a factor of 3 and 2, respectively. Using published permeability coefficients the calculated volume ratio of water expected at cathode and anode lies between 1 (humidified gases) and 1.5 (dry gases). In the present work using dry feed gases, the amount of collected water changes over time at OCV (Fig. 3), from an initial ratio $V_{cathode}/V_{anode}$ of around 6, to a ratio close to 2 after 150 h. Experimental values are thus always >1.5, indicating that effects other than the direct combi-
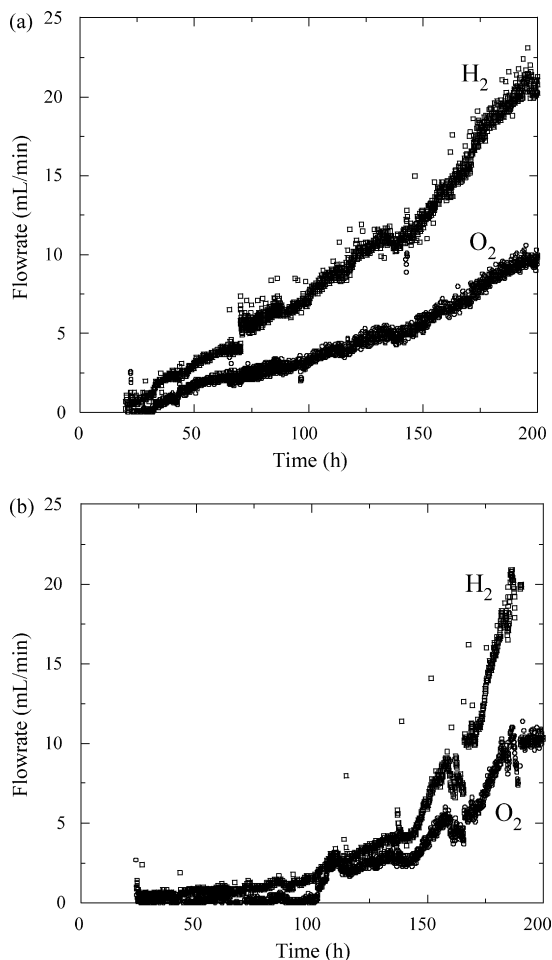

Fig. 2. Dependence of hydrogen crossover current density with time at open circuit. $T_{cell} = 80$ °C, H_2/O_2, gases humidified at 30 °C.

Fig. 4. Consumption of H_2 and O_2 upstream of the fuel cell under open circuit, $T_{cell} = 80\,^\circ C$: (a) gases hydrated at $80\,^\circ C$ and (b) dry gases.

nation of hydrogen and oxygen at the electrodes contribute to water formation, transport and its distribution between the electrodes.

The rate of consumption of hydrogen by the fuel cell at open circuit, from total water collected at the electrodes, and from the hydrogen crossover current (Figs. 2–4) is calculated as $5.6 \times 10^{-6}\,mol\,H_2\,s^{-1}$, $8.3 \times 10^{-6}\,mol\,H_2\,s^{-1}$ and $1.3 \times 10^{-7}\,mol\,H_2\,s^{-1}$, respectively. While the first two of these values lie within reasonable range of each other, the rate of consumption of hydrogen calculated from hydrogen crossover current is smaller by a factor of 40–60. This observation is readily rationalised since electrochemical determination of membrane permeability supposes complete transfer of hydrogen from anode to cathode, and the calculation based on this determination does not consider the possibility of reaction at sites other than the electrodes (e.g. consumption of hydrogen by reduction of platinum ions that have migrated within the membrane).

3.2. Characterisation of product water

Product water at the anode and cathode side was analysed for its fluorine, platinum and sulfur contents, and the results are given in Table 1. Sulfur and platinum were below the limits of detection, but fluorine is found to be present in large amounts, the source of which is fluorine-containing species derived and eluted from the Nafion® membrane or from ionomer present in the electrodes. The results show the concentration of this fluorine is some 2–3 times higher when the feed gases are hydrated, presumably since

Table 1
Elemental analysis of total product water at anode and cathode sides after 100 h at open circuit at a cell temperature of $80\,^\circ C$

	F (ppm)	S (ppm)	Pt (ppm)
Dry gases			
Anode	14	<10	<0.05
Cathode	13	<10	<0.05
Hydrated gases			
Anode	36	<10	<0.05
Cathode	29	<10	<0.05

fluorine-containing fragments are more readily washed out from the membrane under these conditions. Fluorine concentrations are approximately equal at the anode and cathode product water, irrespective of whether the feed gases are hydrated or not.

The negative ion electrospray mass spectra of water collected at the anode and cathode are shown in Fig. 5. The cell providing this water was maintained at $80\,^\circ C$ with hydrated H_2 and O_2 and is thus richer in fluorine-containing fragments (cf. Table 1). The spectra contain 7 main signals that are, in decreasing m/z, at 341, 297, 277, 99, 97, 93 g/charge in both anode and cathode product water, and a signal at m/z 180 g/charge in cathode water, 175 g/charge in anode water. The heaviest fragments are assigned to the molecular ion perfluoro-(3-oxapentane)-4-carboxylic-1-sulfonate: $HO_2CCF(CF_3)O(CF_2)_2SO_3^-$ (I), its decarboxylated derivative $CCF(CF_3)O(CF_2)_2SO_3^-$ and a fragment derived from the dianion of I by loss of a CO_2F moiety. Similar fragments were detected in Fenton (H_2O_2/Fe^{2+}) media [15] used to chemically degrade Nafion®-117 membranes by free radical attack, which confirms the role of radicals in the chemical degradation of Nafion®-112 at high cell potential. A species of 341 g/charge was also identified in the water used to extract degradation products from an MEA based on Flemion® after 150 h at open circuit voltage at $120\,^\circ C$ [23].

These fragments containing carboxylic fragments all derive from end-group degradation of the Nafion® polymer chains. However, at lower m/z, the signal at 97 g/charge is indicative of degradation not of the main chain, but at the pendant groups of the polymer, since it can be assigned to sulfate HSO_4^- (the weak signal at 99 g/charge arising from this ion containing isotope ^{34}S) derived from the sulfonic acid functions on Nafion® side chains. Furthermore, the signal at 180 g/charge could correspond to a side chain fragment $-(CF_2)_2SO_3^-$. This is the first direct evidence of chemical degradation of Nafion pendant groups at high cell potential. Prior to the present work, indirect evidence had been described by Resnick [24] who found that the fluoride emission rate in ex situ experiments in a Fenton medium does not tend to zero when plotted against the number of chain-end groups, which implies
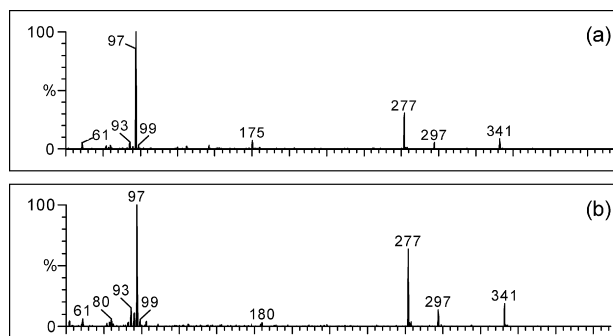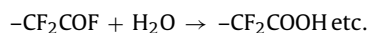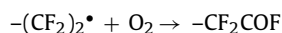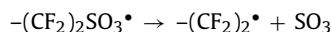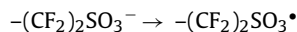

Fig. 5. Negative ion electrospray mass spectra of water collected at the (a) anode and (b) cathode of an MEA aged at OCV under H_2 and O_2. $T_{cell} = 80\,^\circ C$, gases hydrated at $80\,^\circ C$.

that fluoride emission is not only a consequence of degradation of the main chain through an "unzipping" mechanism. Indeed the degradation mechanism suggested [24] commences by oxidation of tetrafluoroethylene sulfonate through:

$$-(CF_2)_2SO_3^- \rightarrow -(CF_2)_2SO_3^\bullet$$

$$-(CF_2)_2SO_3^\bullet \rightarrow -(CF_2)_2^\bullet + SO_3$$

$$-(CF_2)_2^\bullet + O_2 \rightarrow -CF_2COF$$

$$-CF_2COF + H_2O \rightarrow -CF_2COOH \text{ etc.}$$

A recent XPS analysis of Nafion®-112 after ex situ ageing in Fenton solution detected loss of fluorine and sulfur from the membrane, and formation of oxygen-rich moieties in the membrane [25], and HF, H_2O_2, CO_2, SO, SO_2, H_2SO_2 and H_2SO_3 have been detected in the cathode outlet gas produced in open circuit conditions [26]. Much of the previous work has relied upon ion chromatography to follow fluoride emission rate (FER). Some conclusions appear contradictory, in particular the influence of gas hydration in increasing or not the FER, however all authors concur that membrane degradation is favoured by high cell potential and the presence of oxygen [21,27,28]. Although these previous studies have attempted to correlate in situ and ex situ observations with only limited success, there is here close similarity between the degradation fragments identified in the present work following performance loss in situ by OCV hold, and those of ex situ experiments in a Fenton solution, giving strong evidence that in situ degradation of the perfluorosulfonic acid polymer occurs by free radical attack.

3.3. Microscopic characterisation of aged MEAs

MEAs were observed by SEM following in situ ageing for different periods of time at OCV, different MEA preparation conditions (with and without hot-pressing), with and without gas hydration, at gas entry and exit points as well as in the central region of the assembly. Representative results are described here. Fig. 6 shows the cross-section of an MEA (central zone) after ageing for 50 and 100 h under otherwise identical conditions.

The bright features in the micrographs of Fig. 6 are due to platinum, present not only in the electrodes but also as a clearly imaged platinum band present, under these conditions of operation, at the mid-point of the MEA and which thickens with time at OCV. It should be noted that no platinum was observed within the membrane after 24 h at OCV. The thickness of the membrane, nominally 50 μm for dry Nafion®-112, is ca. 30 μm. Visible to the eye in these images also is the difference in brightness at the anode and cathode, and EDX analysis confirms that after ageing at OCV the amount of platinum at the cathode is lower than that of a reference unused MEA, while the amount of platinum at the anode is higher. The overall shift in Pt concentration at cathode (lower) and anode (higher) appears in contrast to conclusions that Pt oxidation can also take place at the anode, giving Pt(II) species that migrate into the membrane [29].

First reports of platinum migration subsequent to fuel cell operation at high cell potential relate to phosphoric acid fuel cells (PAFC). In 1984, the results of Rutherford back-scattering on PAFC electrodes indicated transfer of the vanadium/platinum catalyst from the cathode to the anode. In subsequent work, platinum was detected by EDX in the H_3PO_4 electrolyte after 1500 h of operation, an increase in platinum particle size at the cathode was observed, and the high cell voltage (0.7–1.0 V) implicated as a cause. Since 2005 and during the course of the present work, several publications have described similar observations in PEMFC
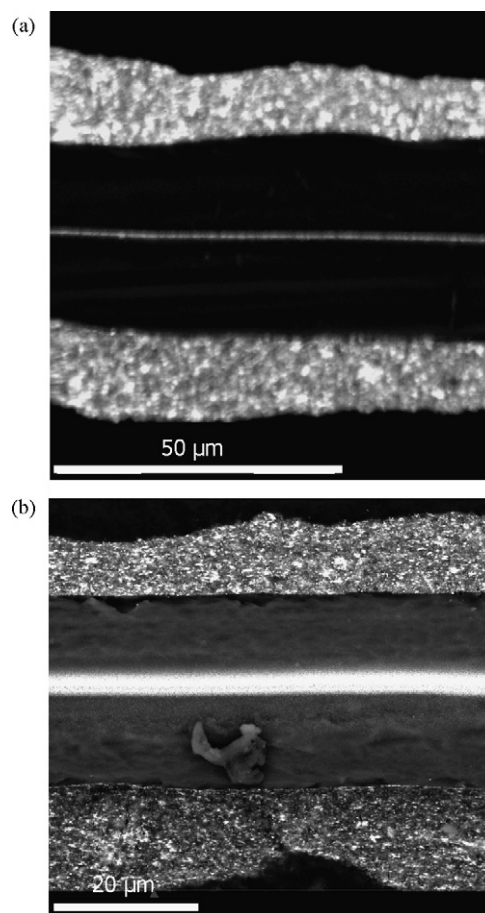

Fig. 6. Scanning electron micrographs of Nafion®-112-based MEAs aged at OCV at 80 °C under H_2 and O_2, 1 bar absolute pressure, gases hydrated at 80 °C. (a) 50 h at OCV and (b) 100 h at OCV.

[10,13]. The phenomenon of platinum dissolution, migration and re-precipitation was indeed modelled in the simulations of Darling and Meyers [30]. In the presence of oxygen or water and at higher potential, PtO is formed and can dissolve as Pt(II). Above 1.2 V, a surface layer of PtO_2 passivates platinum against dissolution [31]. Recent studies by Wang indicate that an equilibrium concentration of dissolved platinum from a Pt/C electrode is reached after 48 h at 0.9 V in 0.57 M perchloric acid electrolyte [32]. The observations of the present work, as described in Figs. 1 and 6, show that when the equilibrium regime is reached after the initial rapid performance loss, platinum particles have already precipitated and assembled as a band in the membrane.

Scanning electron micrographs of an MEA aged for 100 h at OCV in the region of gas inlet, gas outlet, and central zone (cell design comprises co-flow of H_2 and O_2 and serpentine flow fields) are displayed in Fig. 7. In each case, platinum can be observed in the gas diffusion layer at the anode side, indicating significant migration (no platinum is observed in the gas diffusion layer at the cathode side). A measure of the migration of platinum from the cathode to the anode was obtained by EDX, the signal from which was converted to a number of Pt atoms within a given surface area. The results, Table 2 shows that platinum migration from cathode to anode occurs in each of the three areas sampled (gas inlet, central active area, gas outlet), and is severest at the region of gas entry. Interestingly, the total platinum detected (anode + cathode) is similar in each region. Although there is a noticeable difference in thickness of the catalyst layers at the gas inlet (thicker) and
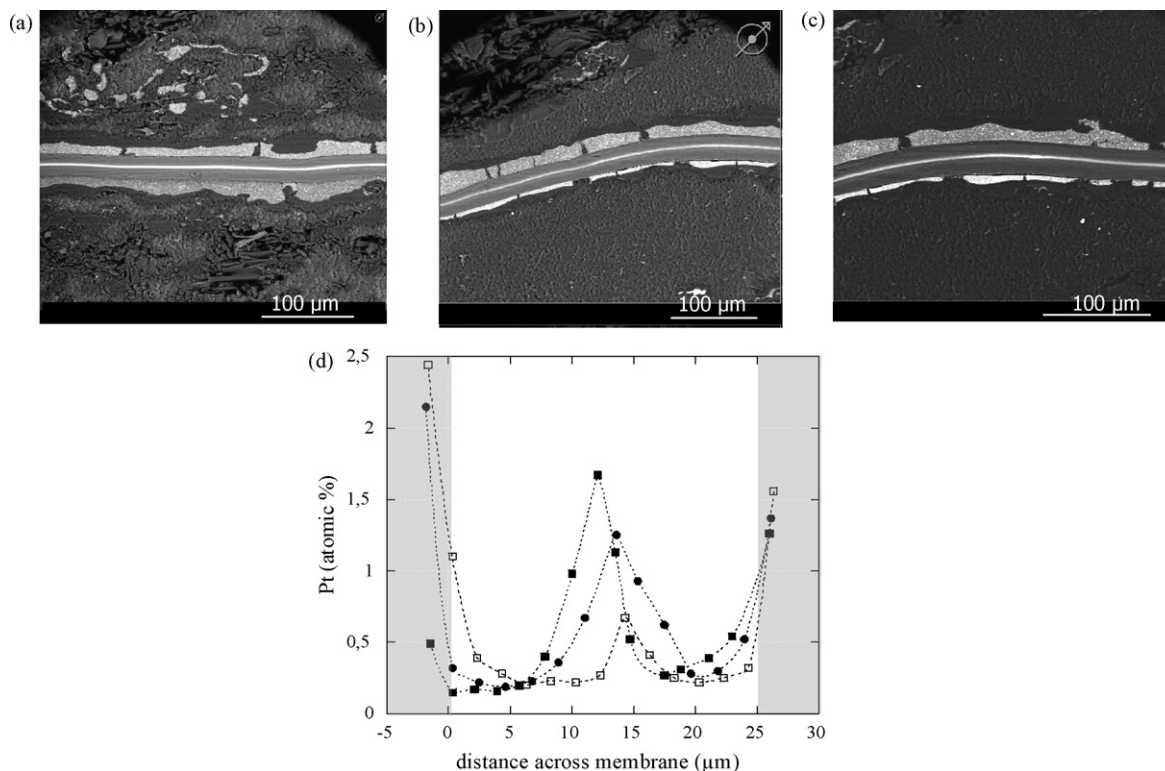
Fig. 7. Scanning electron micrographs of an MEA aged for 100 h at OCV, H_2/O_2, 1 bar absolute pressure, gases hydrated at 80 °C, T_{cell} = 80 °C, in the regions of (a) gas entry (b) central MEA (c) gas exit. Anode is uppermost in these micrographs (d) corresponding plot of Pt content across the membrane thickness from EDX analysis. (■) Pt at gas inlet; (□) Pt at gas outlet; (●) Pt at centre of MEA.

gas outlet (thinner) regions, higher residual cathode platinum is detected in the gas exit region than at the gas entry point. Transfer of platinum from the cathode catalyst layer to the anode was previously described only for an MEA cycled between 0.1 and 1.2 V under nitrogen atmosphere, i.e. in the absence of hydrogen [33].

The platinum precipitation front in the membrane appears more distinctly in the region of gas entry, than at the central or gas exit regions. EDX was again used to quantify these observations across the thickness of the MEA, and the results are plotted in Fig. 7d. It is important to note that although a peak of platinum content is observed in the membrane in each case, corresponding to the Pt band clearly visible in SEM, in fact platinum is detected throughout the thickness of the membrane. The peak of platinum content is highest in the gas inlet region, followed by the centre of the active area, followed by the gas exit region, results that follow the trends of Table 2 with respect to the relative amounts of residual platinum at the cathode in each case. Yu et al. have reported more severe loss of performance in the fuel entry region than in the fuel exit region of an aged MEA and the observations related to greater membrane thinning at the fuel inlet [34]. In the present work, after the 100 h at OCV, 70% of the platinum originally in the cathode catalyst layer in the region of gas entry has migrated into the membrane as positively charged species of platinum(II), where it effectively

charge-balances two perfluorosulfonate side-chains of the Nafion® polymer, with obvious implications on increasing membrane electrical resistance, decreasing electrochemical surface area at the electrodes, and loss of performance (Fig. 1).

To further characterise the morphology of the "Pt band" within the membrane, investigation using transmission electron microscopy was undertaken. The micrographs in Fig. 8 are of a MEA aged for 50 h at OCV (H_2/O_2, 80 °C, gases hydrated at 80 °C), where the Pt band is seen equidistant from the electrodes. At the cathode side, an accumulation of Pt particles is visible at the mem-
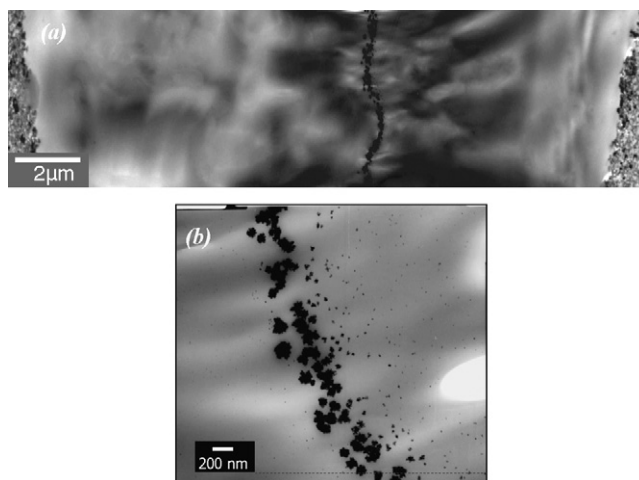

Fig. 8. TEM micrographs of an MEA aged for 50 h at OCV, H_2/O_2, 1 bar absolute pressure, T_{cell} = 80 °C, gases hydrated at 80 °C. (a) MEA cross-section showing cathode, membrane and anode (magnification 2000×); (b) magnification 20k to show the platinum precipitation front in the membrane.

Table 2
Normalised EDX analysis for platinum at anode and cathode in regions of an MEA aged for 100 h at OCV, H_2/O_2, 1 bar absolute pressure, T_{cell} = 80 °C in the vicinity of gas entry, gas exit and central active area

Platinum content (atom % μm^2)	Gas entry	Centre active area	Gas exit
Cathode	8	12	14
Anode	26	22	23

Corresponding SEM micrographs are shown in Fig. 7.

anode   cathode
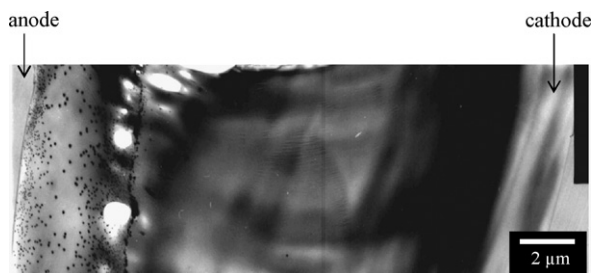

2 µm

Fig. 9. TEM micrograph of an MEA aged for 100 h at OCV, H_2/O_2, $P_{O_2} = 1.5$ bar, $P_{H_2} = 1$ bar, $T_{cell} = 80\,°C$, gases hydrated at $80\,°C$. Magnification 2000×. Anode at left-hand side.

brane/electrode interface (Fig. 8a). At higher magnification, Fig. 8b, the precipitation front is observed to be made up of aggregates of primary particles, each with an appearance characteristic of dendritic growth. However, the platinum front is not symmetrical at its anode and cathode sides, with significant difference in the size of the particles at the anode (larger) and cathode (smaller) sides. Particle growth, not unexpectedly, is most highly developed on the side of the precipitation front in contact with crossover hydrogen gas. In addition, isolated particles (at the anode side) or small aggregates (cathode side) are dispersed throughout the membrane. In all cases, the particles observed are of size greater than those initially present in the electrodes.

Other recent work has described the precipitation of platinum in fuel cell membranes, most often as a Pt band [10,11,33,35], but also as dispersed particles distributed throughout the membrane [36]. Since oxygen (or water) is needed for platinum dissolution, and hydrogen required for platinum precipitation, the position of the precipitation front clearly depends on the operation conditions of the fuel cell, as demonstrated by the TEM micrograph of Fig. 9, where the MEA was maintained at OCV for 100 h with a differential pressure between anode and cathode of 0.5 bar ($P_{O_2} > P_{H_2}$). Under these conditions, the precipitation front is displaced towards the anode, as predicted by the calculations of Darling and Meyers [37], and the distribution of platinum particles and their size is different from when equal pressures are applied at anode and cathode. Thus in Fig. 9 numerous small platinum particles are aggregated between the Pt band and the anode, with significant accumulation at the membrane/anode interface. On the other hand, when the direction of pressure differential is switched ($P_{H_2} \gg P_{O_2}$), no platinum band is detected in the membrane, dissolution and reprecipitation of platinum occurring predominantly within the cathode.

3.4. X-ray spectroscopic characterisation of platinum in MEA aged under OCV

The Pourbaix diagram for Pt shows that at high potential and at low pH, metallic platinum can be oxidised to PtO that can in turn be oxidised to PtO_2, however no direct identification of the nature of the platinum species present in the membrane of an aged MEA has been reported to date. X-ray photoelectron spectroscopy (XPS) is a highly suited probe technique for determination of Pt oxidation state and, in principle, for analysis across the thickness of an aged MEA when analysis is alternated with cycles of abrasion. Until now, although XPS has been used to examine the electrodes of aged MEAs [38], no previous XPS study has been made of the membrane of an MEA aged in situ. In the present work, the aged MEA was examined by SEM prior to XPS analysis to ensure the presence of platinum in the form of a precipitated band. Experiments were performed by beginning analysis at the cathode side and alternating analysis and abrasion and, on a second adjacent sample taken from the same aged MEA, by beginning analysis at the anode side and alternating

analysis and abrasion cycles. As abrasion cycles progressed however, the sample was observed to change colour, becoming white, while the binding energies characteristic of elements present in the Nafion® membrane shifted, probably due to surface charging. The polymer component of the MEA thus appears unstable under the X-ray beam of the experiment, as was previously described by Schulze et al. [39] in their XPS study of a pristine Nafion® membrane. Platinum, however, was undamaged by the X-ray beam, and XPS spectra were recorded until the support material at the anode side was detected, after a period of ca. 140 min. Starting XPS analysis and detection from the side of the membrane that had been in contact with the cathode, no platinum was detected in the initial scans. After 48 min of abrasion, the XPS spectrum contained signals in the binding energy range 70–80 eV, characteristic of platinum. The spectrum is complex, contributions being given by Pt $4f_{7/2}$ and Pt $4f_{5/2}$ in each case, in a ratio of relative intensity roughly 3–2. The double contribution of each platinum species to the spectrum increases the level of confidence in the results obtained by simulating the experimental spectra. After 78 min of argon abrasion signals from Pt(0) and Pt(II) are observed and, after 93 min a further contribution to the spectrum is given by Pt(IV). No Pt(IV) was detected in unused commercial electrodes. A previous XPS study of the catalyst layers of in-house prepared electrodes identified Pt(II) and Pt(IV) in both fresh and used electrodes [40], suggesting that the oxidised platinum was a product of fabrication and not of ageing.

The experimental spectrum recorded after 93 min of abrasion, and the corresponding simulation, including contributions from Pt(0), Pt(II) and Pt(IV), is shown in Fig. 10a, and the concentration profile of each of these species is plotted as a function of the abrasion time in Fig. 10b. The experiment was then repeated starting detection and abrasion at the anode side, and the observations confirmed the conclusions that the polymer and the platinum band are eroded at different rates, the polymer component degrading under the X-ray beam, and that Pt(0), Pt(II) and Pt(IV) species co-exist in the "platinum band". Because of the different rates of erosion of Pt and Nafion®, one of the original aims of the experiment which was to map the nature of Pt species across the membrane, could not be achieved. On the other hand, the relative positions of the various platinum species can be discussed.

If Fig. 10b is considered in more detail, on progressing from the cathode side to the anode side of the membrane, when platinum is first detected, it is present as both Pt(0) and Pt(II), while Pt(IV) is detected at a point more distant from the cathode. From the Pourbaix diagram, it is known that Pt(IV) is formed at higher cell potentials than are needed for Pt(II). Such a situation would correspond to the first hours in OCV regime, since thereafter the cell performance has declined to lower potentials (Fig. 1), and Pt is oxidised to Pt(II) but not beyond. A different mechanism must therefore be sought to reconcile the identification of Pt(IV), surmised here to involve the oxidation of Pt(II) by hydrogen peroxide. H_2O_2 can be generated within the membrane by two-electron reduction of permeated oxygen by hydrogen on the catalytic sites of precipitated Pt particles ($O_2 + 2H^+ + 2e^- = H_2O_2$; $E_0 = 0.695$ V). The Pt band is formed at a position where the theoretical potential profile in the membrane changes from that of the cathode side (ca. 1 V) to that of the anode side (ca. 0 V) and the potential requirement for H_2O_2 formation is satisfied. Formation of H_2O_2 at the anode catalyst by reduction of fully crossed over oxygen [18] and at the cathode catalyst by reaction of oxygen with permeated hydrogen [41] has been suggested by other authors, and H_2O_2 detected electrochemically within the membrane using Pt microelectrodes [18]. The potential at the cathode is however, more positive than that for H_2O_2 formation [5]. Once H_2O_2 is generated within the membrane, it can catalytically decompose on the divalent platinum centres identified by XPS, and give either Pt(IV) species directly,
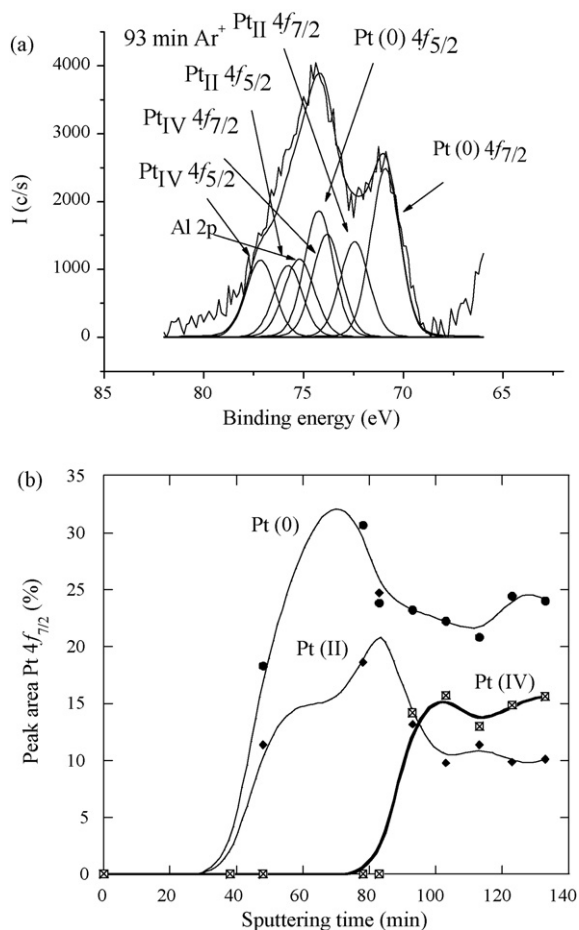
Fig. 10. (a) XPS spectrum after 93 min abrasion of an MEA aged for 90 h under OCV, H_2/O_2, 1 bar absolute pressure, T_{cell} = 80 °C, gases hydrated at 80 °C. (b) Concentration profile of Pt species as a function of abrasion time.

or Pt(III) centres that rapidly disproportionate to Pt(II) and Pt(IV). This process can lead to the production of radical species responsible for chemical degradation of the polymer *within* the membrane, explaining the rapid increase in permeability (hydrogen crossover current) on ageing at OCV. That the Pt band is the principal site for hydrogen peroxide generation is supported by the observations of Ohma et al. that the magnitude of fluoride emission at the anode and the cathode correlated with the location of the platinum band closer to the anode or cathode, respectively [11]. Mittal et al. has observed that the fluoride emission rate from an aged MEA is comparable whether or not an anode catalyst is used [27], which is inconsistent with a mechanism involving H_2O_2 production only at the anode. Finally, it can be deduced from Fig. 10(b) that the concentration of metallic and oxidised platinum species in the membrane are equal throughout the region of the membrane in which platinum is detected. This observation provides an additional handle for estimation of the primary size of the platinum particles. Considering that the particles comprise a metallic core and oxidised surface, the surface/volume ratio (dispersion) is 1/2, providing a primary particle size of 2 nm from the empirical relation $d = 10 /D$ (d: particle diameter; D: dispersion). This particle size is compatible with that observed in TEM, e.g. in Fig. 9. Ionic platinum was also identified in the decantation solution used to extract soluble species from the membrane of an aged MEA using UV spectrophotometry [35]. However this study appears inconclusive because Pt(II) and Pt(IV) were also detected in the extract from the membrane of a fresh MEA assembled with electrodes developed in-house.

It has been shown unequivocally by Inaba et al. that H_2O_2 is produced by oxygen reduction on Pt/C catalysts loaded on glassy carbon in 1 M $HClO_4$, and that the amount of hydrogen peroxide increases with a decrease in loading density of Pt/C [42]. These authors concluded that the 2-e⁻ reduction pathway, which is negligible on a clean, bulk Pt surface [43], exists intrinsically on Pt particles supported on carbon. On the other hand, Watanabe et al. [21] have convincingly demonstrated that a PFSA membrane in which Pt particles have been formed by ion-exchange and reduction (Pt-PFSA) has lower FER than an unmodified PFSA, which these authors have attributed to the catalytic scavenging of H_2O_2 and/or radical species by the metallic Pt sites. The unambiguous difference between Pt-PFSA membranes prepared by ion-exchange and reduction, and those resulting from in situ MEA ageing is the existence of oxidised Pt in the latter, Pt(0) and Pt(II) being always detected simultaneously in the membrane of an aged MEA. The presence of Pt(II) in the surface layer of Pt nanoparticles is considered to prevent the metallic platinum core from playing the role of radical scavenger.

4. Conclusion

This work has shown that the degradation products in water produced by a Nafion®-based MEA operating at high cell potential are the same as those identified by ex situ accelerated ageing of Nafion membranes in Fenton solutions, providing good evidence for a degradation mechanism implicating free radicals. It has identified Pt(II) and Pt(IV) in the membrane for the first time, and has proposed explanations for their origins. XPS also shows that when Pt(IV) is present in the membrane, Pt(II) occurs in equal amounts, an observation entirely consistent with a mechanism in which Pt(IV) is generated by disproportionation of Pt(III) produced in the reaction of Pt(II) with hydrogen peroxide. Under the high potential and low pH conditions initially present, platinum dissolves from the cathode and migrates through the membrane, some even completely traversing the membrane and enriching the platinum content at the anode. Platinum also precipitates throughout the membrane as particles of primary particle size 2 nm and forms a platinum front appearing as a platinum band at the point at which the hydrogen and oxygen gas pressures are equilibrated. At equal hydrogen and oxygen partial pressures, the platinum band precipitates in the centre of the membrane, whereas with higher oxygen partial pressure, the band is displaced towards the anode, and with higher hydrogen partial pressure (or when air is used as oxidant), dissolved platinum is reprecipitated within the cathode, or at the membrane–cathode interface. In situ monitoring of hydrogen crossover indicates that not all the hydrogen supplied by the anode is used in water production, an observation that supports partial consumption of hydrogen within the membrane by reduction of migrating platinum ions. Platinum is formed, at least after the first ca. 50 h of ageing at OCV, as Pt(II). X-ray photoelectron spectroscopy has provided irrefutable evidence however not only for Pt(II) but also for Pt(IV) that could be formed, it is surmised, via the oxidation of Pt(II) by hydrogen peroxide. This reaction could lead to the generation within the membrane of peroxide radicals that attack the Nafion® polymer, both at the chain ends, and at the pendant functional groups since fragments of both degraded end-group and degraded side-group species have been identified in product water from negative ion spray mass spectrometry.

References

[1] D.J. Jones, J. Rozière, J. Membr. Sci. 185 (2001) 41.
[2] J. Rozière, D.J. Jones, Annu. Rev. Mater. Res. 33 (2003) 503.
[3] M.A. Hickner, H. Ghassemi, Y.S. Kim, B.R. Einsla, J.E. McGrath, Chem. Rev. 104 (2004) 4587.
[4] J. Péron, E. Ruiz, D.J. Jones, J. Rozière, J. Membr. Sci. 314 (2008) 247.
[5] R. Borup, J. Meyers, B. Pivovar, Y.S. Kim, R. Mukundan, N. Garland, D. Myers, M. Wilson, F. Garzon, D. Wood, P. Zelenay, K. More, K. Stroh, T. Zawodzinski, J. Boncella, J.E. McGrath, M. Inaba, K. Miyatake, M. Hori, K. Ota, Z. Ogumi, S. Miyata, A. Nishikata, Z. Siroma, Y. Uchimoto, K. Yasuda, K.-i. Kimijima, N. Iwashita, Chem. Rev. 107 (2007) 3904.
[6] F.A. De Bruijn, V.A.T. Dam, G.J.M. Janssen, Fuel Cells 8 (2008) 3.
[7] D.E. Curtin, R.D. Lousenberg, T.J. Henry, P.C. Tangeman, M.E. Tisack, J. Power Sources 131 (2004) 41.
[8] J. Aragane, T. Murahashi, T. Odaka, J. Electrochem. Soc. 135 (1988) 844.
[9] M.S. Wilson, F.H. Garzon, K.E. Sickafus, S. Gottesfeld, J. Electrochem. Soc. 140 (1993) 2872.
[10] P.J. Ferreira, G.J. la O', Y. Shao-Horn, D. Morgan, R. Makharia, S. Kocha, H.A. Gasteiger, J. Electrochem. Soc. 152 (2005) A2256.
[11] A. Ohma, S. Suga, S. Yamamoto, K. Shinohara, J. Electrochem. Soc. 154 (2007) B757.
[12] J. Peron, D.J. Jones, Rozière, ECS Trans. 11 (Proton Exchange Membrane Fuel Cells 7, Part 1) (2007) 71.
[13] P. Yu, M. Pemberton, P. Plasse, J. Power Sources 144 (2005) 11.
[14] H.R. Colon-Mercado, B.N. Popov, J. Power Sources 155 (2006) 253.
[15] J. Healy, C. Hayden, T. Xie, K. Olson, R. Waldo, M. Brundage, H. Gasteiger, J. Abbott, Fuel Cells 5 (2005) 302.
[16] V.O. Mittal, H.R. Kunz, J.M. Fenton, J. Electrochem. Soc. 153 (2006) A1755.
[17] M. Inaba, T. Kinumoto, M. Kiriake, R. Umebayashi, A. Tasaka, Z. Ogumi, Electrochim. Acta 51 (2006) 5746.
[18] W. Liu, D. Zuckerbrod, J. Electrochem. Soc. 152 (2005) A1165.
[19] S. Hommura, K. Kawahara, T. Shimohira, Y. Teraoka, J. Electrochem. Soc. 159 (2007) A29.
[20] F. Finsterwalder, M. Quintus, M. Schalsoke, T. Guth, G. S Frank, Abstract No. 485 210th ECS Meeting, Los Angeles, 2006.
[21] M. Aoki, H. Uchida, M. Watanabe, Electrochem. Commun. 8 (2006) 1509.
[22] T. Sakai, H. Takenaka, N. Wakabayashi, Y. Kawami, E. Torikai, J. Electrochem. Soc. 132 (1985) 1328.
[23] S. Hommura, K. Kawahara, T. S Shimohira, Abstract No. 803, 207th ECS Meeting, Quebec City, Canada, 2005.
[24] P. Resnick, seminar, ENSCM, Montpellier, France, 2007.
[25] C. Chen, G. Levitin, D.W. Hess, T.F. Fuller, J. Power Sources 169 (2007) 288.
[26] K. Teranishi, K. Kawata, S. Tsushima, S. Hirai, Electrochem. Solid-State Lett. 9 (2006) A475.
[27] V.O. Mittal, H.R. Kunz, J.M. Fenton, Electrochem. Solid-State Lett. 9 (2006) A299.
[28] E. Endoh, S. Terazono, H. Widjaja, Y. Takimoto, Electrochem. Solid-State Lett. 7 (2004) A209.
[29] J. Xie, D.L. Wood III, K.L. More, P. Atanassov, R.L. Borup, J. Electrochem. Soc. 152 (2005) A1011.
[30] R.M. Darling, J.P. Meyers, J. Electrochem. Soc. 150 (2003) A1523.
[31] V.A.T. Dam, F.A. de Bruijn, J. Electrochem. Soc. 154 (2007) B494.
[32] X. Wang, R. Kumar, D.J. Myers, Electrochem. Solid-State Lett. 9 (2006) A225.
[33] K. Yasuda, A. Taniguchi, T. Akita, T. Ioroi, Z. Siroma, Phys. Chem. Chem. Phys. 8 (2006) 746.
[34] J. Yu, T. Matsuura, Y. Yoshikawa, M. Nazrul Islam, M. Hori, Phys. Chem. Chem. Phys. 7 (2005) 373.
[35] E. Guilminot, A. Corcella, F. Charlot, F. Maillard, M. Chatenet, J. Electrochem. Soc. 154 (2007) B96.
[36] T. Akita, A. Taniguchi, J. Maekawa, Z. Siroma, K. Tanaka, M. Kohyama, K. Yasuda, J. Power Sources 159 (2006) 461.
[37] R.M. Darling, J.P. Meyers, J. Electrochem. Soc. 152 (2005) A242.
[38] M. Schulze, A. Schneider, E. Gulzow, J. Power Sources 127 (2004) 213.
[39] M. Schulze, M. Lorenz, N. Wagner, E. Gulzow, Fresenius J. Anal. Chem. 365 (1999) 106.
[40] C. Huang, K.S. Tan, J. Lin, K.L. Tan, Chem. Phys. Lett. 371 (2003) 80.
[41] T. Kinumoto, M. Inaba, Y. Nakayama, K. Ogata, R. Umebayashi, A. Tasaka, Y. Iriyama, T. Abe, Z. Ogumi, J. Power Sources 158 (2006) 1222.
[42] M. Inaba, H. Yamada, J. Tokunaga, R. Umebayashi, A. Matsuzawa, A. Tasaka, Abstract No. 1196, 210th ECS Meeting, Los Angeles, 2006.
[43] N.M. Markovic, H.A. Gasteiger, P.N. Ross, J. Phys. Chem. 99 (1995) 3411.